NASA CR-165272

(NASA-CR-165272) COPLANAR BACK CONTACTS FOR THIN SILICON SOLAR CELLS Final Report, 24 Jul. 1978 - 15 Jul. 1980 (Solarex Corp., Rockville, Md.) 38 p HC A03/MF A01 CSCL 10A

N81-18495

Unclas
G3/44 41499

COPLANAR BACK CONTACTS

FOR

THIN SILICON SOLAR CELLS

G. Storti, A. Scheinine, D. Whitehouse
J. Wohlgemuth, C. Wrigley, and M. Giuliano

Solarex Corporation
1335 Piccard Drive
Rockville, MD 20850
(301) 948-0202

Final Report

Covering the Period From

July 24, 1978 to July 15, 1980

prepared for

National Aeronautics and Space Administration
NASA-Lewis Research Center
Cleveland, OH 44135

Contract NAS3-21250

SOLAREX CORPORATION

NASA CR-165272

COPLANAR BACK CONTACTS

FOR

THIN SILICON SOLAR CELLS

G. Storti, A. Scheinine, D. Whitehouse
J. Wohlgemuth, C. Wrigley, and M. Giuliano

Solarex Corporation
1335 Piccard Drive
Rockville, MD 20850
(301) 948-0202

Final Report

Covering the Period From

July 24, 1978 to July 15, 1980

prepared for

National Aeronautics and Space Administration
NASA-Lewis Research Center
Cleveland, OH 44135

Contract NAS3-21250

1. Report No.	2. Government Accession No.	3. Recipient's Catalog No.
CR-165272		

4. Title and Subtitle	5. Report Date
Coplanar Back Contacts for Thin Silicon Solar Cells	January 1981
	6. Performing Organization Code

7. Author(s)	8. Performing Organization Report No.
G. Storti, A. Scheinine, D. Whitehouse, J. Wohlgemuth, C. Wrigley, and M. Giuliano	
	10. Work Unit No.

9. Performing Organization Name and Address	11. Contract or Grant No.
Solarex Corporation 1335 Piccard Drive Rockville, MD 20350	NAS3-21250

12. Sponsoring Agency Name and Address	13. Type of Report and Period Covered
National Aeronautics and Space Administration Washington, DC 20546	FINAL REPORT July 1978 to Dec. 1980
	14. Sponsoring Agency Code

15. Supplementary Notes

Project Manager: Cosmo R. Baraona, NASA-Lewis Research Center, Cleveland, Ohio 44135

16. Abstract The type of coplanar back contact solar cell described in this report was constructed with interdigitated n^+ and p^+ type regions on the back of the cell, such that both contacts are made on the back with no metallization grid on the front. This cell construction has several potential advantages over conventional cells for space use--namely, convenience of interconnects, lower operating temperature and higher efficiency due to the elimination of grid shadowing. However, the processing is more complex, and the cell is inherently more radiation sensitive. The latter problem can be reduced substantially by making the cells very thin (approximately 50 μm).

Two types of interdigitated back contact cells are possible, the types being dependent on the character of the front surface. The front surface field cell has a front surface region that is of the same conductivity type as the bulk but is more heavily doped. This creates an electric field at the surface which repels the minority carriers. The tandem junction cell has a front surface region of a conductivity type that is opposite to that of the bulk. The junction thus created floats to open-circuit voltage on illumination and injects carriers into the bulk which then can be collected at the rear junction. For space use, the front surface field cell is potentially more radiation resistant than the tandem junction cell because the flow of minority carriers (electrons) into the bulk will be less sensitive to the production of recombination centers, particularly in the space charge region at the front surface.

As a consequence of the above considerations and the relative ease of fabrication, the efforts of this program were directed towards the fabrication of a front surface field interdigitated back contact cell. The fabrication efforts were assisted by modeling and analysis intended to pinpoint the major loss mechanisms limiting efficiency.

Efforts to fabricate high efficiency, ultrathin coplanar back contact cells are described. Included is a description of design considerations, cell fabrication, and theoretical and experimental analyses of loss mechanisms. The result of these efforts has been the fabrication of a 11.8% AMO efficient, 50 μm cell when measured at 25° C. Design and process changes required to increase the efficiency and yield are indicated.

17. Key Words (Suggested by Author(s))	18. Distribution Statement
Silicon Solar cells Coplanar contacts	Unclassified-Unlimited

19. Security Classif. (of this report)	20. Security Classif. (of this page)	21. No. of Pages	22. Price*
		iii 34	

*For sale by the National Technical Information Service, Springfield, Virginia 22161

NASA-C-168 (Rev. 10-75)

TABLE OF CONTENTS

LIST OF ILLUSTRATIONS

LIST OF TABLES

1.0 Introduction

The coplanar back contact solar cell (Ref. 1&2) is constructed with interdigitated n^+ and p^+ type regions on the back of the cell, such that both contacts are made on the back with no metallization grid on the front. This cell construction has several potential advantages over conventional cells for space use -- namely, convenience of interconnects, lower operating temperature and higher efficiency due to the elimination of grid shadowing. However, the processing is more complex, and the cell is inherently more radiation sensitive. The latter problem can be reduced substantially by making the cells very thin (approximately 50 μm).

Two types of interdigitated back contact cells are possible, the types being dependent on the character of the front surface. The front surface field cell has a front surface region that is of the same conductivity type as the bulk but is more heavily doped. This creates an electric field at the surface which repels the minority carriers. The tandem junction cell has a front surface region of a conductivity type that is opposite to that of the bulk. The junction thus created floats to open-circuit voltage on illumination and injects carriers into the bulk which then can be collected at the rear junction. For space use, the front surface field cell is potentially more radiation resistant than the tandem junction cell because the flow of minority carriers (electrons) into the bulk will be less sensitive to the production of recombination centers, particularly in the space charge region at the front surface.

As a consequence of the above considerations and the relative ease of fabrication, the efforts of this program were directed towards the fabrication of a front surface field interdigitated back contact cell. The fabrication efforts were assisted by modeling and analysis intended to pinpoint the major loss mechanisms limiting efficiency.

Efforts to fabricate high efficiency, ultrathin coplanar back contact cells are described. Included is a description of design considerations, cell fabrication, and theoretical and experimental analyses of loss mechanisms. The result of these efforts has been the fabrication of a 11.8% AMO efficient, 50 μm cell when measured at 25°C. Design and process changes required to increase the efficiency and yield are indicated.

2.0 Technical Discussion

The objectives of this development program were to explore and assess methods for making interdigitated coplanar back contacts suitable for ultrathin high efficiency silicon solar cells for space use, to fabricate cells by the best method and to identify any areas that require further development. An efficiency goal of 14% AMO was set for cells with a nominal thickness of 50 to 75 micrometers where both n^+ and p^+ contacts were formed on the back of the cell. Simple test structures were to be used where possible for the exploratory effort and methods assessment in Task I, Investigation of Techniques. The Task I effort included design considerations and computer modeling and is described in Section 2.1. The Task II effort encompassed cell fabrication and evaluation and is described in Section 2.2 along with a summary of all cell fabrication efforts.

2.1 Investigation of Techniques

Three principal ares of investigation of techniques were of interest in the development of the coplanar back contact cells. These relate to formation of the front surface field, solar cell design considerations for the optimum arrangement of interdigitated n^+ and p^+ fingers on the back of the cell and computer modeling efforts tying together these two areas of investigation with minority carrier and diffusion length effects in the bulk. Each of these is described in the subsequent subsections.

2.1.1 Front Surface Field Formation

Pyrolytic boron-doped oxide deposition was used to establish the front surface field. Initially, in order to establish a baseline measurement technique, undoped MOS structures were fabricated. Automatic capacitance/conductance bridges for both 1KHz and 1MHz measuring frequencies were employed for capacitance-voltage and conductance-voltage evaluation of the simple MOS structures. The results were used to determine the silicon surface doping concentrations and the oxide-silicon surface interface fast state densities. In addition to the pyrolytic oxide, tantalum oxide was used as an MOS dielectric to exercise measurement of silicon surface potentials. Measurements on MOS capacitors (Al-Oxide-Si-Al) containing either an undoped pyrolytically deposited oxide or Ta_2O_5 were made in order to obtain base line information. Figure 1 shows typical capacitance-voltage results for SiO_2 and Ta_2O_5 structures. The capacitance-voltage curve for the SiO_2 suggests that the conduction band in the p-type silicon bends downward at the SiO_2 - Si interface. Consequently, it appears that substantial recombination at a Si-SiO_2 interface is probable. For the Ta_2O_5, the conduction band is indicated

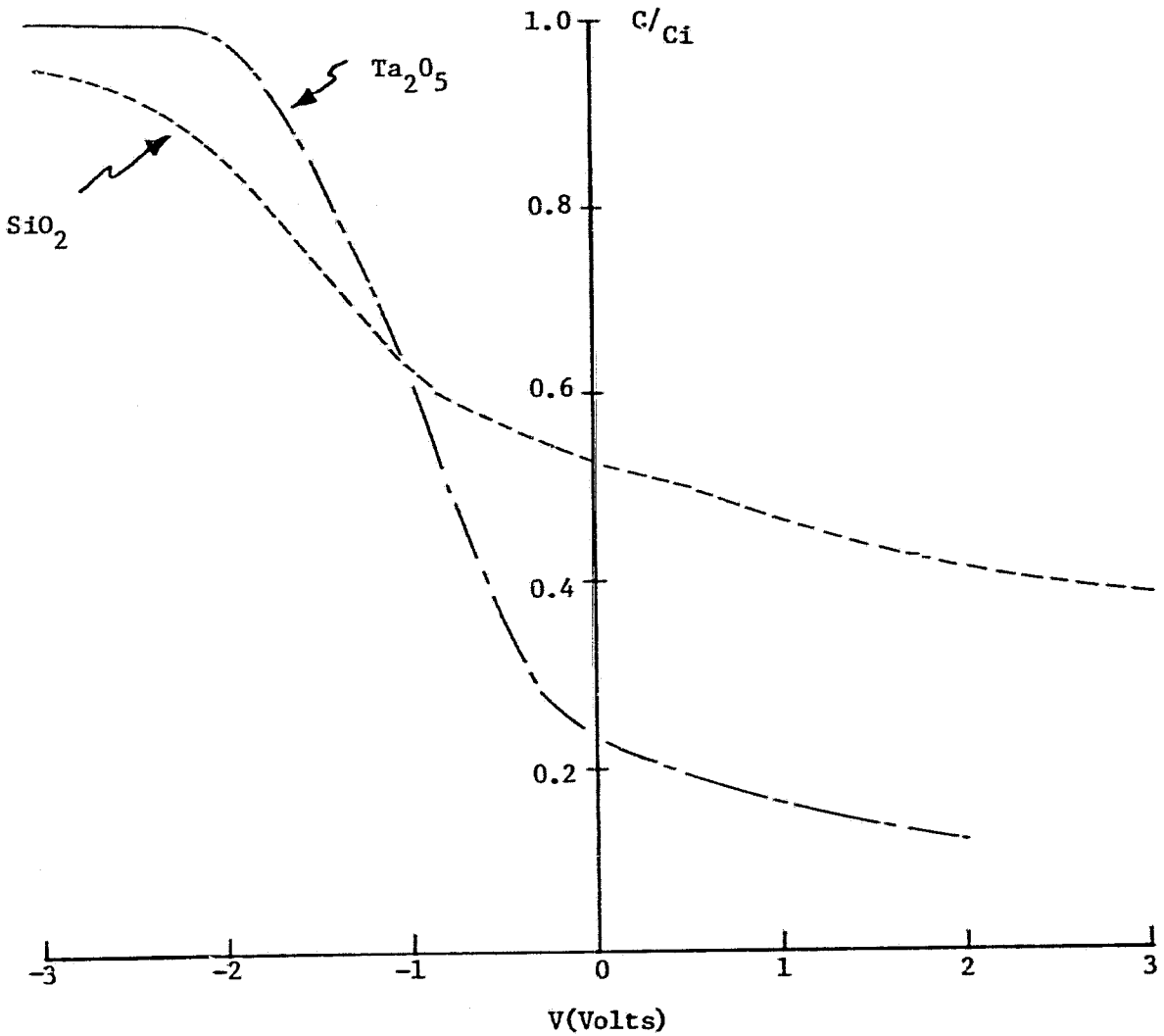

FIGURE 1: C-V dependence of Al-SiO_2-Si-Al and Al-Ta_2O_5-Si-Al MOS capacitors at 1 MHz.

to be flatter as it approaches the Si-Ta_2O_5 interface, and recombination at the interface is correspondingly less likely. However, Ta_2O_5 still does not appear to be capable of lessening surface recombination sufficiently.

A number of wafers containing Al-SiO_2:B-Si-Al MOS structures were then fabricated and measured. The boron doped oxide thickness was between 0.1 and 0.12 μm. The wafers were exposed to temperatures ranging from 700°C to 950°C for ≈ 20 minutes prior to metallization in order to diffuse boron into the silicon. The results of capacitance-voltage measurements are seen in Figure 2. Under the assumption that the diffusion of boron into the silicon with resultant conduction band bending is responsible for the shift of the C-V curves, the results indicated that sufficient boron diffusion was occurring at 800°C and above to form an effective front surface field. Consequently, during cell fabrication, it was concluded that formation of the front surface field could occur at the same time that the n^+ layer is diffused ($T_{diff} \simeq 870°C$).

2.1.2 Design Considerations for the Interdigitated Back-Contact Cell

The basic cell configuration is that as seen in Figure 3. At the cell front, there is the anti-reflection coating and the p^+ diffused region. At the cell back are repeated phosphorus doped n^+, p, aluminum doped p^+, and p regions. The principal loss mechanisms can be readily detailed. For the short-circuit current and open-circuit voltage they are:

- front surface recombination due either to processes in the silicon or at the silicon anti-reflection coating interface.
- recombination in the p-type bulk

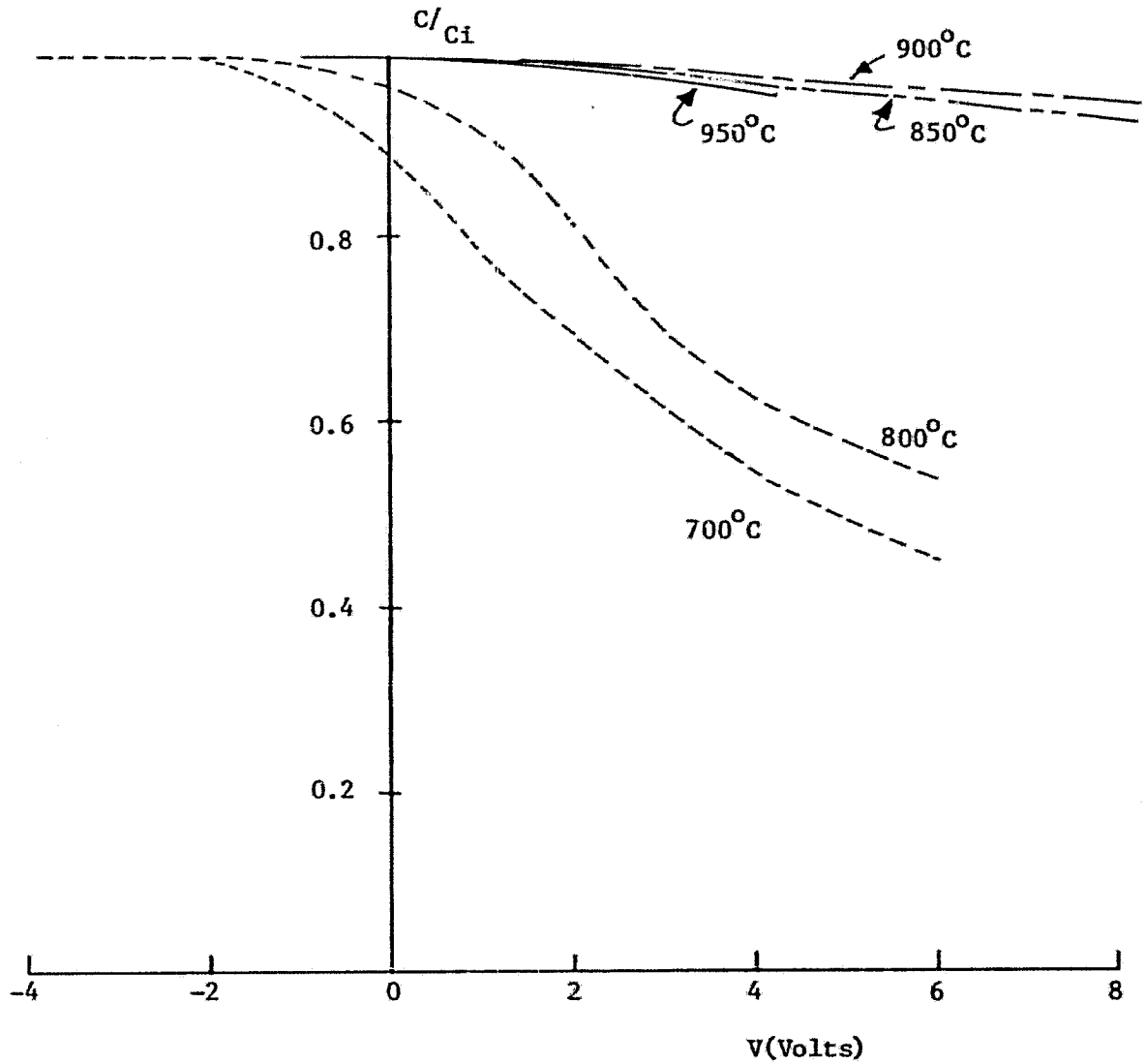

FIGURE 2: C-V dependence of Al-SiO_2:B-Si-Al MOS capacitors. Temperatures indicate the respective diffusion temperatures of the boron doped oxide of the different samples.

- back surface recombination at the p-region surface or in the p^+ region.

For the fill factor, the series resistance and/or shunt resistance is the major potential loss mechanism.

Front surface recombination can be minimized by low temperature diffusion of boron into the silicon and by using high index anti-reflection coating that causes band bending at the surface which repels minority carriers. Tantalum oxide is an anti-reflection material that does this.

Recombination in the bulk can be minimized by using starting material with a high lifetime and by utilizing cell fabrication processes that do not degrade lifetime. Also, the influence of the bulk recombination can be reduced by utilizing thin silicon slices (e.g., 50 μm thick).

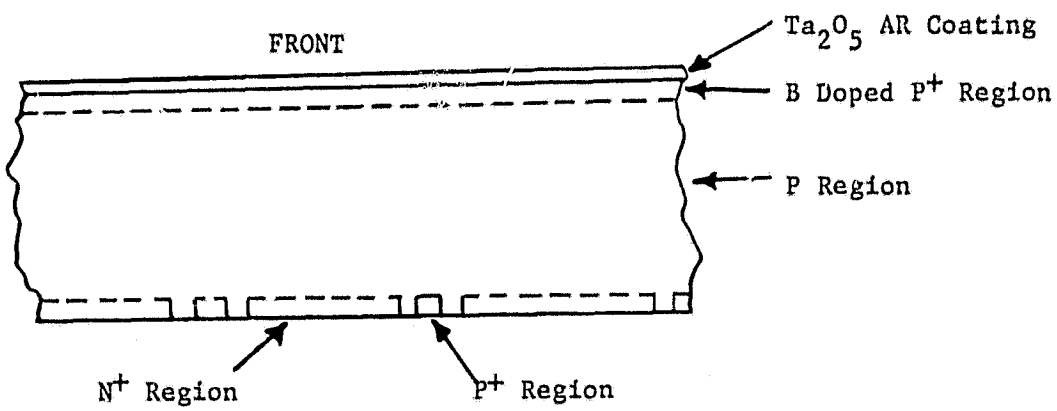

Figure 3. CROSS-SECTION OF A COPLANAR-BACK-CONTACT CELL

Back surface recombination at the p and p^+ surface can be reduced primarily by minimizing the back surface area containing these regions -- that is, the n^+ diffused region should be maximized.

In summary, the combination of low front surface recombination, high index anti-reflection coating, high bulk lifetime, thin wafers and a maximized back n^+ region should lead to high short-circuit currents and open-circuit voltages. In fact, with low front surface recombination and a maximized back n^+ region, the effect of the bulk lifetime on the short-circuit current and open-circuit voltage is diminished for very thin cells. When the minority carrier diffusion length, L_n, exceeds the width of the gap between n^+ regions the open-circuit voltage is enhanced because the reverse saturation current is decreased (minority carriers injected into the bulk will re-inject into the n^+ region before recombining). This phenomenon is similar to that seen in vertical junction cells(Ref. 3).

Series resistance can affect the fill factor of the cells, but it is possible to have a more heavily diffused n^+ region and wider contacts because they are located on the back. The n^+ area is maximized consistent with adequate p^+ contact area and minimum p-surface. Too narrow a p-region can result in lateral shunting, but is desirable from the standpoint of minimizing back surface recombination velocity.

2.1.3 Computer Modeling and Analysis

During the course of the cell fabrication efforts, a computer model of the cell was developed and a number of measurements were made in order to determine the principal loss mechanisms. Since maximizing, the current

produced by the cells also leads to a maximization of the open-circuit voltage and efficiency, the analysis efforts were concentrated on the short-circuit current.

The computer model used the relaxation method on a two dimensional lattice of points. (See Appendix for a more detailed description of the relaxation method). The boundary condition on the front surface is a given surface recombination velocity. The p^+ region and the back p region between the fingers are also modeled by assigning hypothetical surface recombination velocities. The n^+ region boundary is taken at the edge of the depletion region in the bulk. For short circuit current the n^+ boundary condition is zero excess minority carriers.

After the relaxation method was used to calculate the distribution of minority carriers in the bulk, the short circuit current was calculated from the minority carrier gradient at the junction that bounds the n^+ region.

The calculation of photogeneration rates in the silicon bulk takes into account the variation of absorption coefficient with wavelength. Thus the photogeneration rates from front to back are realistically modeled. The computer model assumes that there are no reflection losses since the computer derived short circuit current can be scaled to any assumed wavelength independent absorption.

The results of the computer modeling show a maximum surface recombination velocity that must not be surpassed in order to achieve high efficiency. Roughly speaking, this maximum is 100 cm/sec. Three surfaces must be considered: the front surface, the p^+ region of the back surface, and the region between the contacts, which we shall call the p-region. The short circuit current changes as surface recombination velocity is varied

as shown in Figure 4 and 5. In both figures I_{sc} is drawn as a function of the front surface recombination velocity. In Figure 4 the p^+ surface recombination velocity effect is shown by drawing three curves for V_{s,p^+} = 100, 1,000 and 10,000 cm/sec. The case of V_{s,p^+} = 10 cm/sec is nearly identical to the 100 cm/sec case. In Figure 5 the three curves represent variations of the p-region surface recombination velocity, $V_{s,p}$. The same three values are used, $V_{s,p}$ = 100, 1,000 and 10,000 cm/sec. Also, for this graph the curve for $V_{s,p}$ = 10 cm/sec would be nearly identical to the curve for V_s = 100 cm/sec.

In comparing Figure 4 and Figure 5 it can be seen that the loss of current as $V_{s,p}$ is changed from 100 to 1,000 cm/sec is not as great as the same change in V_{s,p^+}. This is consistent with what one would expect for the particular configuration being considered, i.e., 13-1 - 5-1. The numbers stand for a 13 mil wide n^+ region, a 5 mil wide p^+ region, and one mil p-region between the two regions. Hence the ratio of p^+ area to p area is 5/2, and consequently the cell is more sensitive to variations in the p^+ surface recombination velocity than the rear p-surface recombination velocity.

The finger geometry was subsequently improved by going from 13-1-5-1 to 16-1-2-1. The non-junction area to total area was thereby decreased from 7/20 (35%) to 4/20 (20%). For this geometry the effect of recombination in the bulk was studied with the computer model. The results are shown in Table I. As expected, when the diffusion length approaches the cell thickness, or less, a substantial decrease in the short-circuit current occurs.

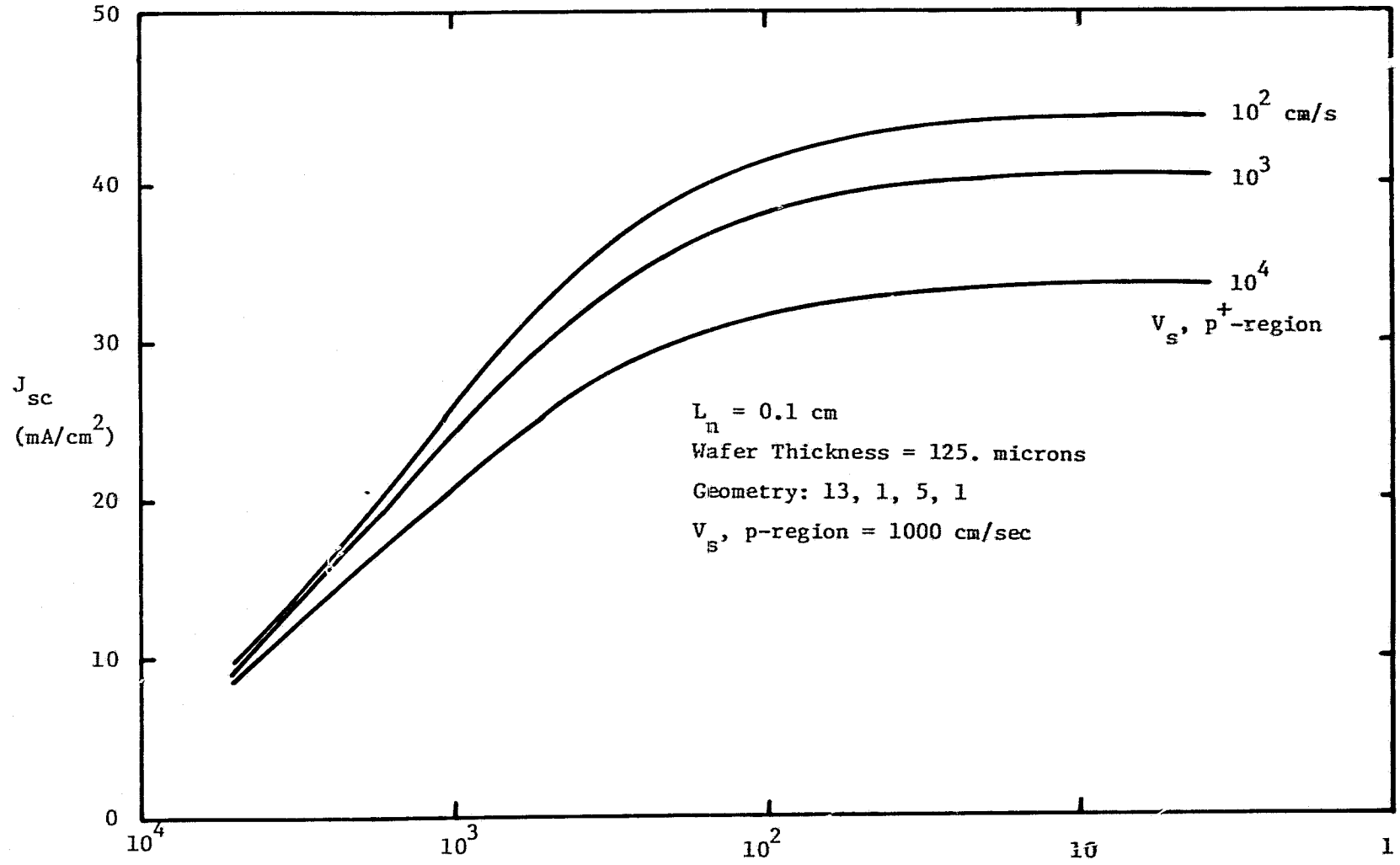

FIGURE 4. V_s Front Surface (cm/sec)

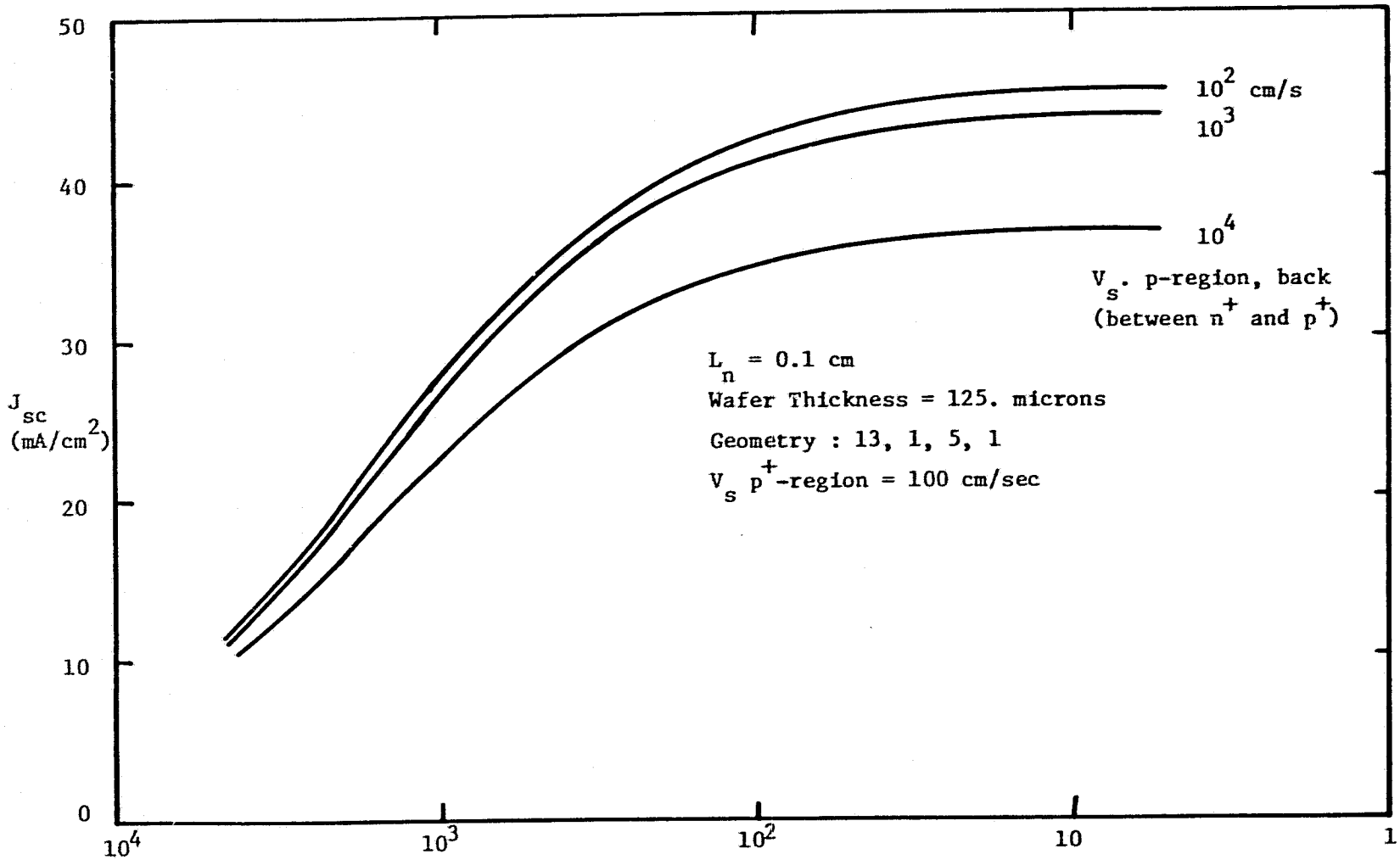

FIGURE 5. V_s Front Surface (cm/sec)

TABLE I

The Effect of Minority Carrier Diffusion Length

On Short Circuit Current Density

No Reflection Losses are Assumed

Geometry:

n^+ p^+

16 - 1 - 2 - 1 (mils); 3 mil thick

Recombination Velocity:

(cm/sec)

p : 1000.

p^+ : 100.

front : 4. & 100.

L_n (cm)	CURRENT (mA/cm^2)	
	4.	100.=V_s front (cm/sec)
.1	44	43
.05	44	43
.03	43	42
.02	41	40
.015	39	37-1/2
.01	33	32

2.2 Cell Fabrication and Evaluation

The process sequence developed for this cell is shown in Figure 6 After thinning with a NaOH etch, a boron doped silicon dioxide layer is deposited on the front of the slice and an un-doped oxide layer on the back. In a series of photolithography steps, portions of the back oxide are removed for phosphorus diffusion and high-low p^+ - p junction formation with evaporated Al as the source. The resultant n^+ and p^+ regions are then metallized with Ti-Pd-Ag to provide contacts to the cell. The front oxide is then removed and a Ta_2O_5 anti-reflection coating applied.

In the course of the cell fabrication efforts, three different cell thicknesses (50 μm, 75 μm, and 125 μm) and three different mask patterns for the back diffused regions (16 mil-n^+, 1 mil-p^+, 2 mil-p^+, 1 mil-p; 13 mil-n^+, 1 mil-p, 5 mil-p^+, 1 mil-p; and 5 mil-n^+, 5 mil-p, 5 mil-p^+, 5 mil-p) were investigated. The thinnest cell and the 16-1-2-1 diffused region configuration were chosen in order to maximize efficiency. This diffused region configuration of the cell back is shown in Figure 7.

2.2.1 Cell Fabrication Chronology

To obtain base line information, undoped oxides were pyrolytically deposited on 125 μm thick Si wafers using the 5-5-5-5 geometry.* Figure 8 curve 1 shows the I-V curve of the best cell from this effort (AMO efficiency equals 2.9% at 25°C). When the oxide layer was removed from other cells from this lot, J_{sc} decreased from ≃ 10 mA/cm^2 to ≃ 2 mA/cm^2. A Ta_2O_5 anti-reflection coating did not increase the current density above that expected from the change in the reflectance. Next, a set of cells was fabricated with boron doped SiO_2 on the front and undoped SiO_2 on the back. Figure 8 curve 2 shows the I-V curve for the best cell in this group.

*5 mil n^+, 5 mil p, 5 mil p^+, 5 mil p

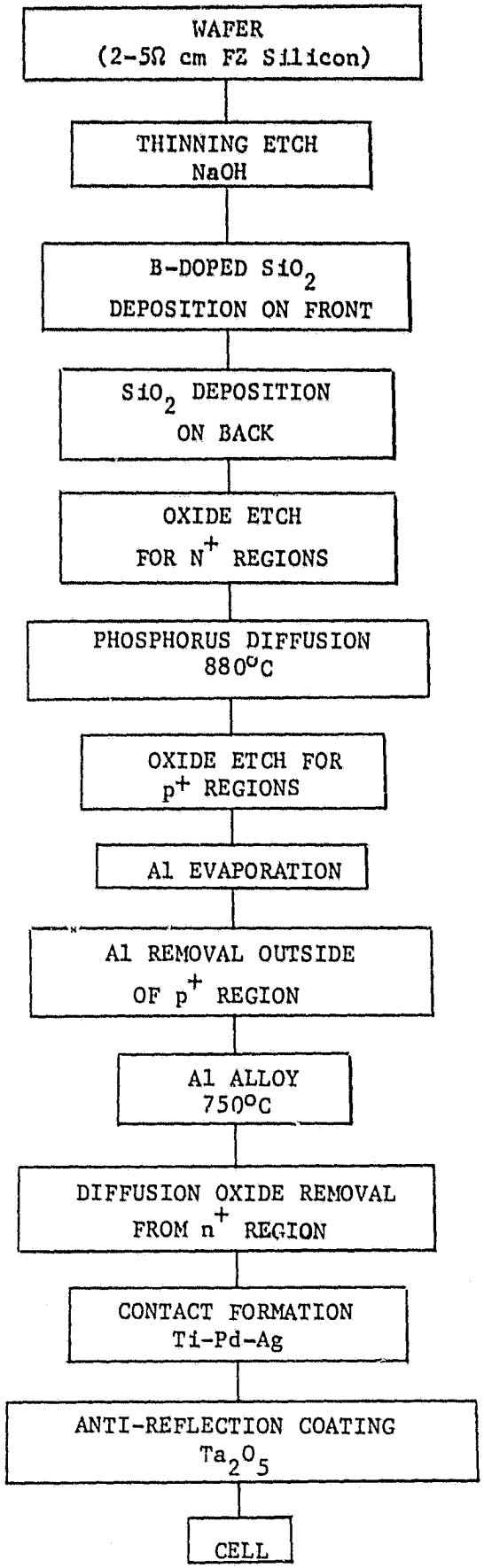

FIGURE 6: PROCESS SEQUENCE FOR THE COPLANAR BACK-CONTACT CELL

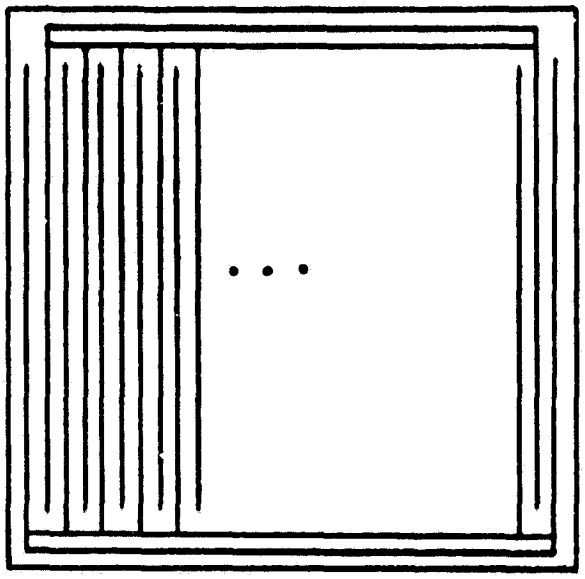

Back of Cell

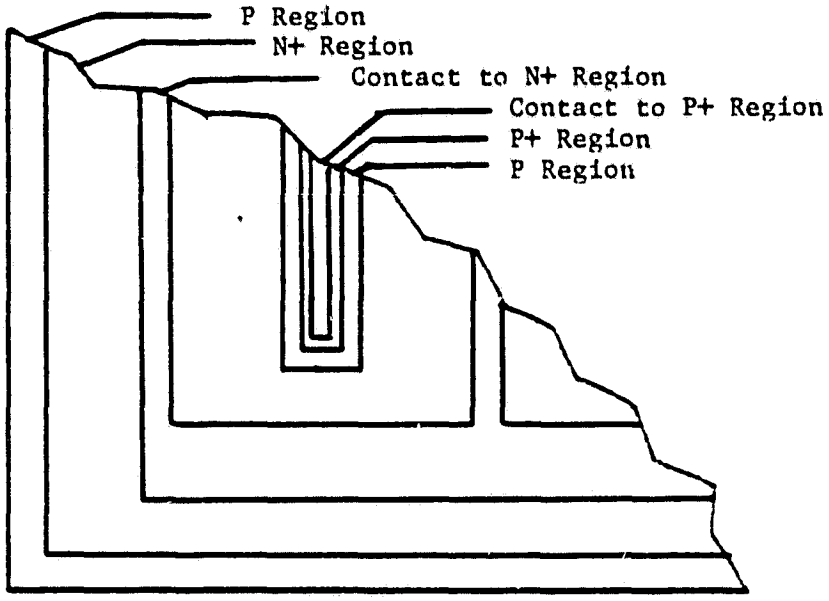

Detail of Back of Cell

N+ Region Width: 16 mils (406 μm)

P+ Region Width: 2 mils (51 μm)

P Region Width: 1 mil (25 μm)

Figure 7. DIFFUSED REGION AND CONTACT CONFIGURATION OF COPLANAR-BACK-CONTACT CELL

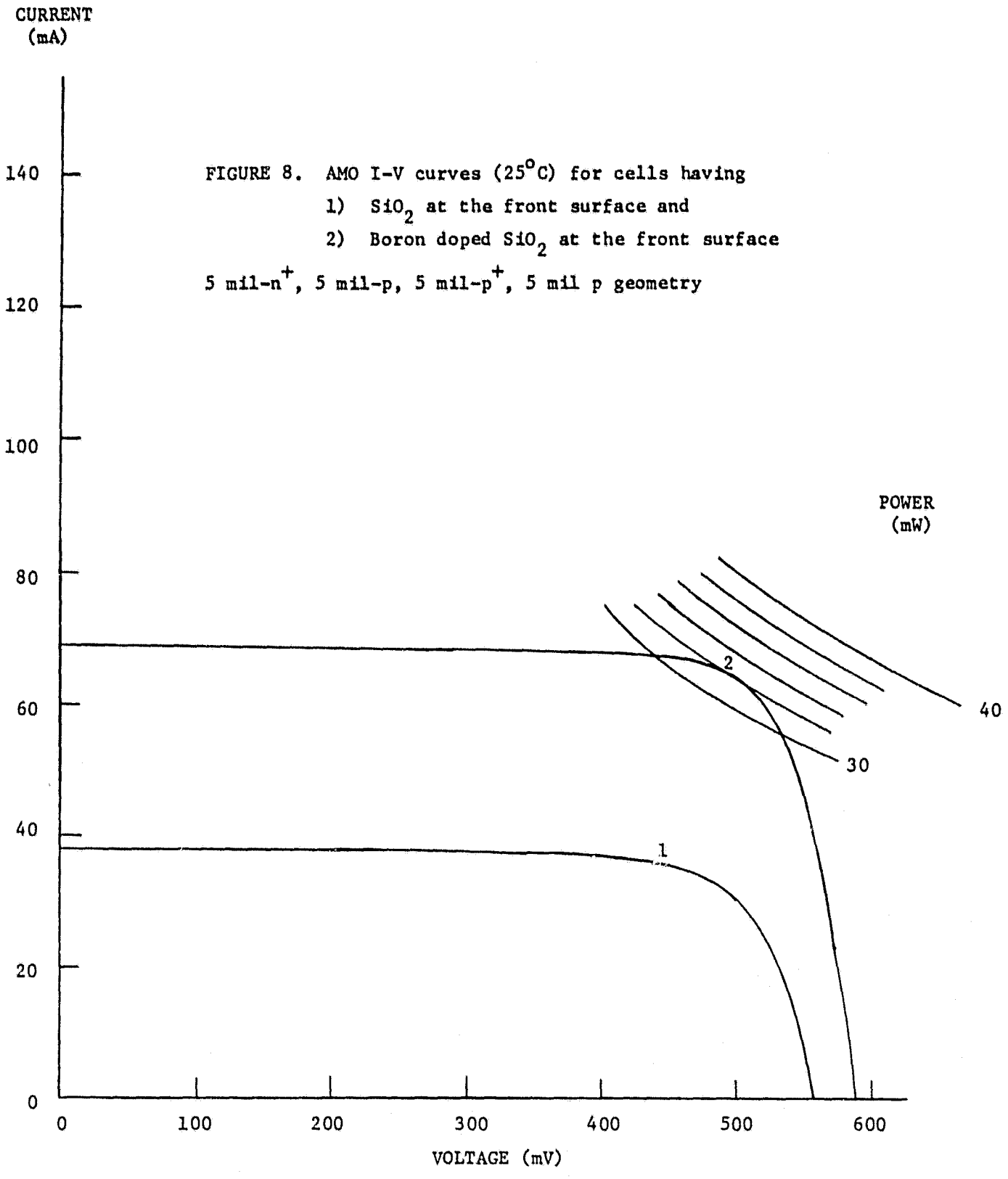

FIGURE 8. AMO I-V curves (25°C) for cells having
1) SiO_2 at the front surface and
2) Boron doped SiO_2 at the front surface
5 mil-n^+, 5 mil-p, 5 mil-p^+, 5 mil p geometry

An AMO efficiency of 5.8% at 25°C was measured. Short-circuit current densities near 17 mA/cm^2 were measured on cells from this group although they had a thick SiO_2:B layer. This layer was partially removed on some cells so as to have a first order anti-reflection coating. J_{sc}'s exceeding 20 mA/cm^2 were then measured.

The internal collection efficiency of the cell shown in Figure 8, curve 2 was calculated from the quantum yield and reflectance and is shown in Figure 9. The response of the cell remains unchanged for wavelengths between 400 nm and 1000 nm. This result suggested that significant recombination was occurring at the SiO_2 - p-region interface at the back of the cell.

The first experiment to reduce the back surface recombination involved the deposition of boron doped SiO_2 over the entire back of the cell, the idea being to create a field at the surface of the p-regions that would repel the minority carriers. An increase in current density to approximately 20 mA/cm^2 was measured for the doped oxide cells. This contrasts with approximately 15 mA/cm^2 for the undoped oxide cells. Although there was an increase in current density, the cells showed poor open circuit voltages (<500 mV) and fill factors. It was believed that the boron doping affected the n^+ regions and further experiments in this direction were terminated.

The second experiment involved the expansion of either the n^+ or p^+ regions so as to minimize the width of the p-regions. Masks were fabricated in-house for this purpose. The new pattern had either 15 mil wide n^+ and 5 mil wide p^+ regions or 15 mil wide p^+ and 5 mil wide n^+ retions. Because there was little or no p-region on the back surface separating the n^+ and

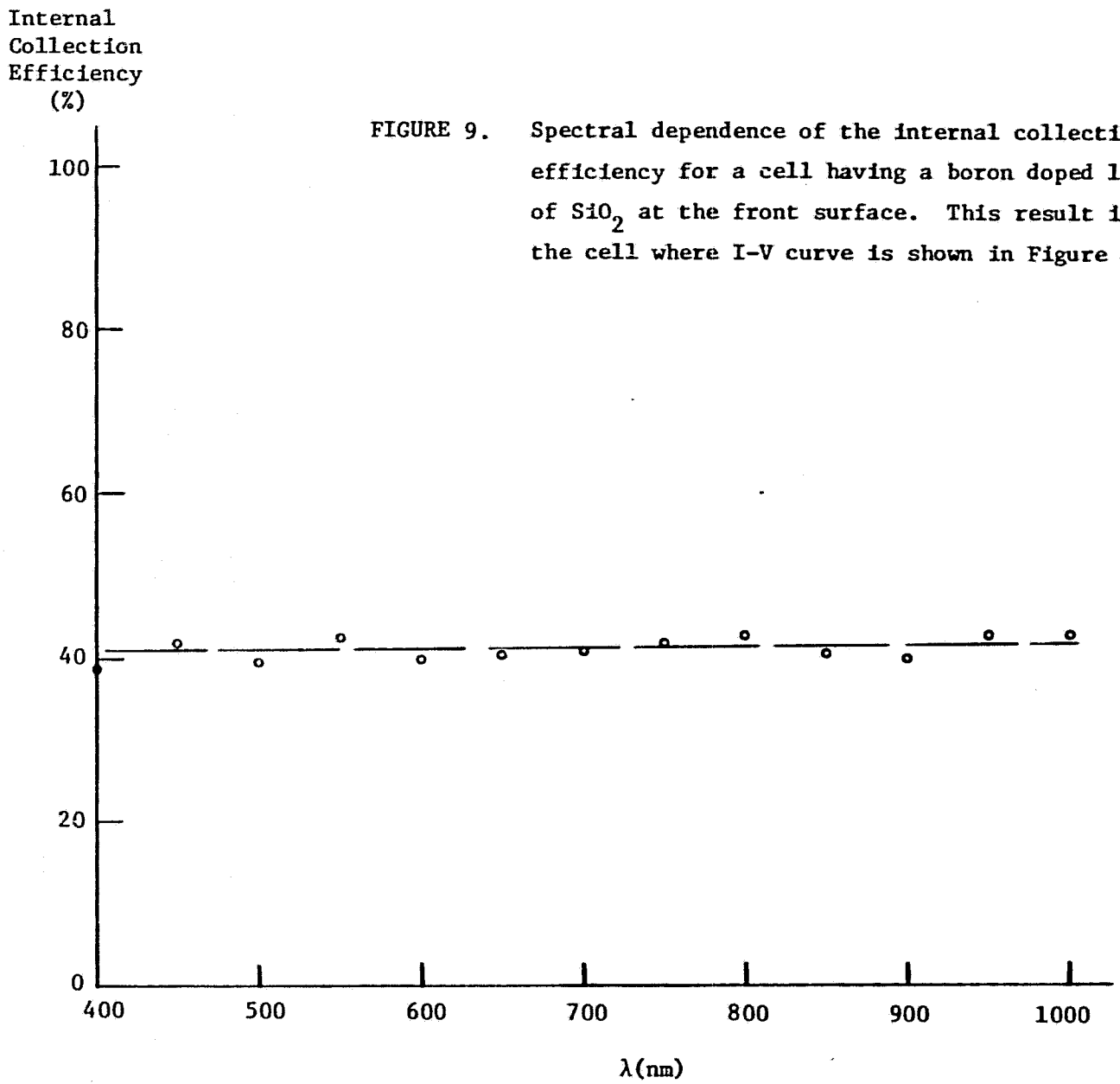

FIGURE 9. Spectral dependence of the internal collection efficiency for a cell having a boron doped layer of SiO_2 at the front surface. This result is for the cell where I-V curve is shown in Figure 8, curve 2.

p^+ regions, it was expected that both V_{oc} and the fill factor would be poor. Cells with expanded n^+ regions were measured to have current densities exceeding 25 mA/cm^2 even with glass front layers having an average reflectance between 25 and 30%. The boron doped SiO_2 layer on one of the cells was etched to first order anti-reflection coating thickness (approximately 10-15% overall reflectance). Cell current density increased from approximately 23 mA/cm^2 to almost 28 mA/cm^2. The I-V curve of this cell is seen in Figure 10. Both quantum yield and reflectance measurements were made on this cell. The results of these measurements are seen in Figure 11. The internal collection efficiency is approximately 70% between 400 nm and 900 nm and increases to 85% at 1000 nm. This indicates that either some front surface recombination is occurring or the minority carrier diffusion length was not large enough and that back surface recombination was substantially reduced.

Expanded p^+ region cells had an average current density approximately one-half that of the expanded n^+ region cells, indicating that this was not a good geometry.

A few 50 μm thick cells were also fabricated in this experiment. For cells having an expanded n^+ region, current densities were equivalent to the 125 μm thick cells (i.e., approximately 22 - mA/cm^2 with the boron-doped glass intact.)

These experiments indicated that considerably different diffused region widths were needed for high efficiency cells. The initial result from the modeling of the effects of surface recombination on cell performance were also obtained at this time. They confirmed that for attainable values of the surface recombination velocity of a p-SiO_2 interface (1000 cm/s),

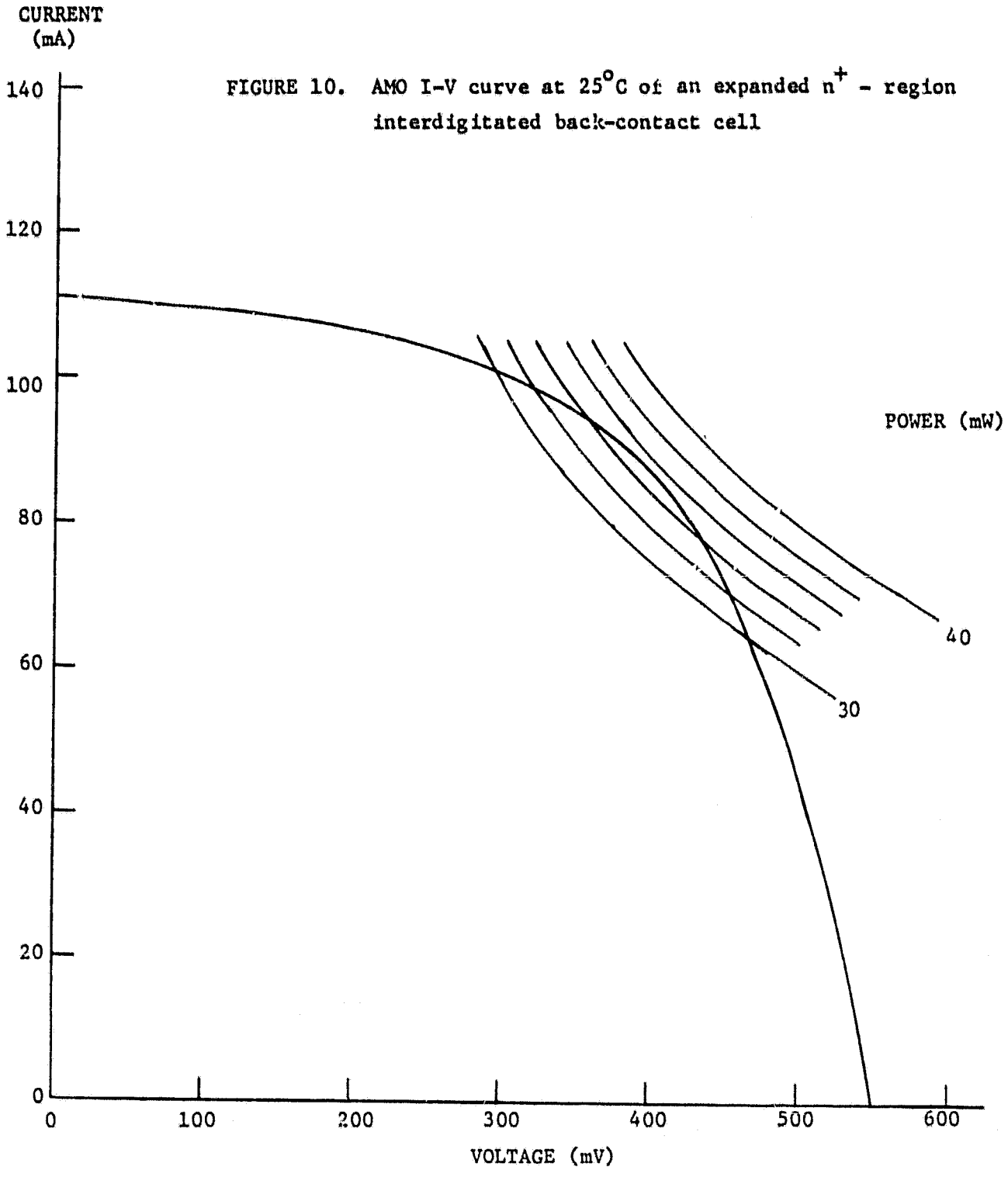

FIGURE 10. AMO I-V curve at 25°C of an expanded n^+ - region interdigitated back-contact cell

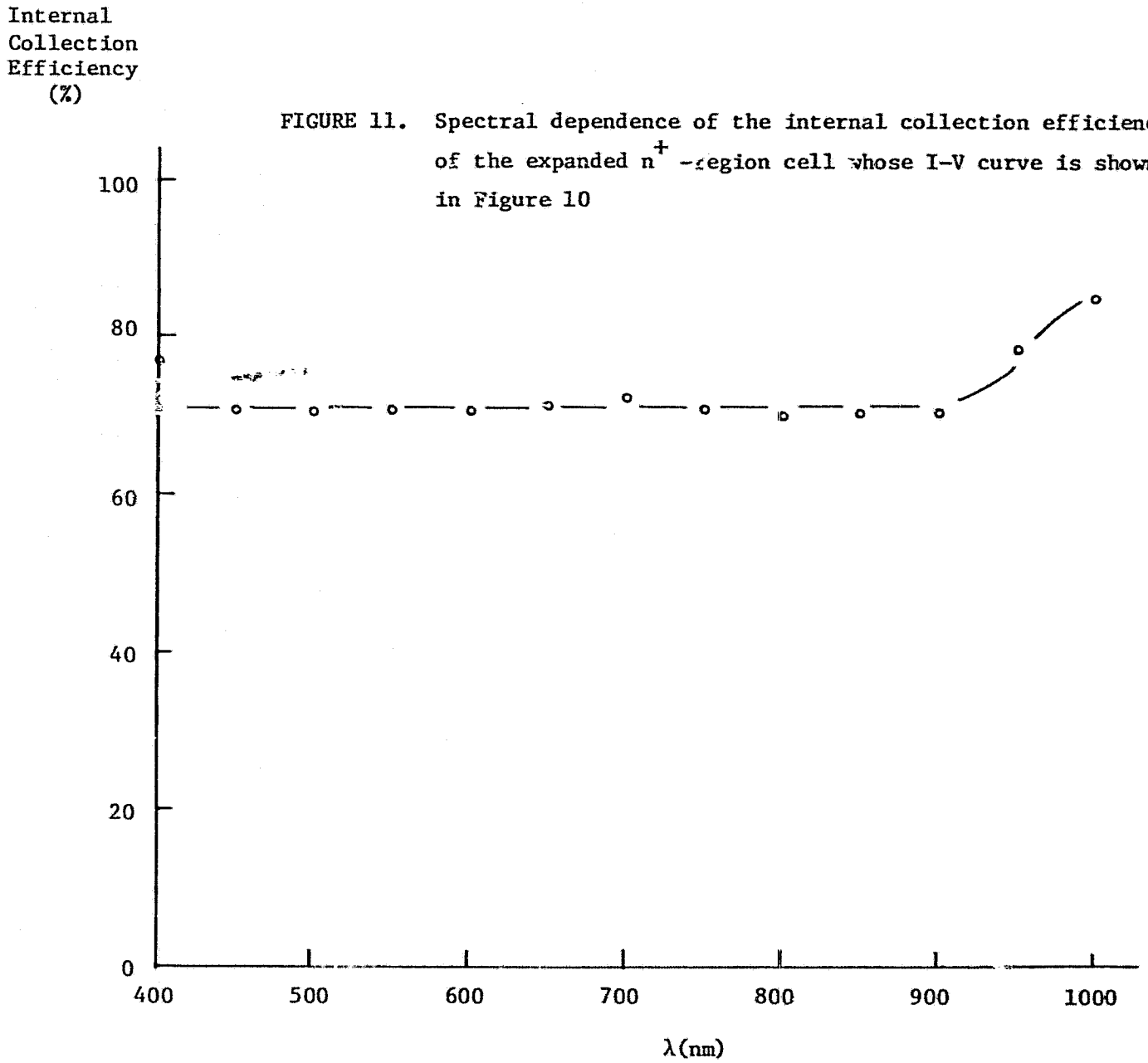

FIGURE 11. Spectral dependence of the internal collection efficiency of the expanded n^+ -region cell whose I-V curve is shown in Figure 10

the width of the back p-regions must be minimized in order to obtain the required current densities ($\simeq$ 40 mA/cm^2). Masks were therefore fabricated to reduce the size of the p-region.

Cells were then fabricated using a 13-1-5-1 (n^+-p-p^+-p) mask configuration. Two ohm-cm Czochralski silicon was thinned to 75 μm thickness and the wafers were diffused at 880°C. The I-V characteristics of the best cell from this effort are seen in Figure 12. The AMO efficiency was 7.0% for a front surface field planar cell with a non-optimized SiO_2 anti-reflection coating. The results on cells using the expanded n^+ region clearly showed the increased current and efficiency expected.

Fabrication efforts continued using the 13-1-5-1 (n^+-p-p^+-p) mask configuration and 1.3Ω-cm float zone silicon. The latter was introduced in order to improve the base lifetime of the device. The silicon was etched to 75 μm thickness, and diffusions were done at 880°C. The boron-doped silicon dioxide on the front surface was stripped, and a spin-on and sintered TaO_x anti-reflection coating was put in its place. The best cells had an AMO power of 52 mW (9.5% efficiency) and a short circuit current density of 29.5 mA/cm^2. Scanning of one of these cells with a 90 μm spot of light showed decreases in the short circuit current above the p and p^+ regions, indicating that recombination was taking place at the p and p^+ surfaces.

At this time, new masks having a 16-1-2-1 (n^+-p-p^+-p) configuration were received, and fabrication commenced using 1.3 Ω-cm float zone silicon of 75 μm thickness. Diffusions were carried out at 880°C. A spin-on TaO_x anti-reflection coating was applied after removal of the SiO_2:B front layer. The best cell fabricated showed AMO power of 60 mW (10.9% efficiency) and

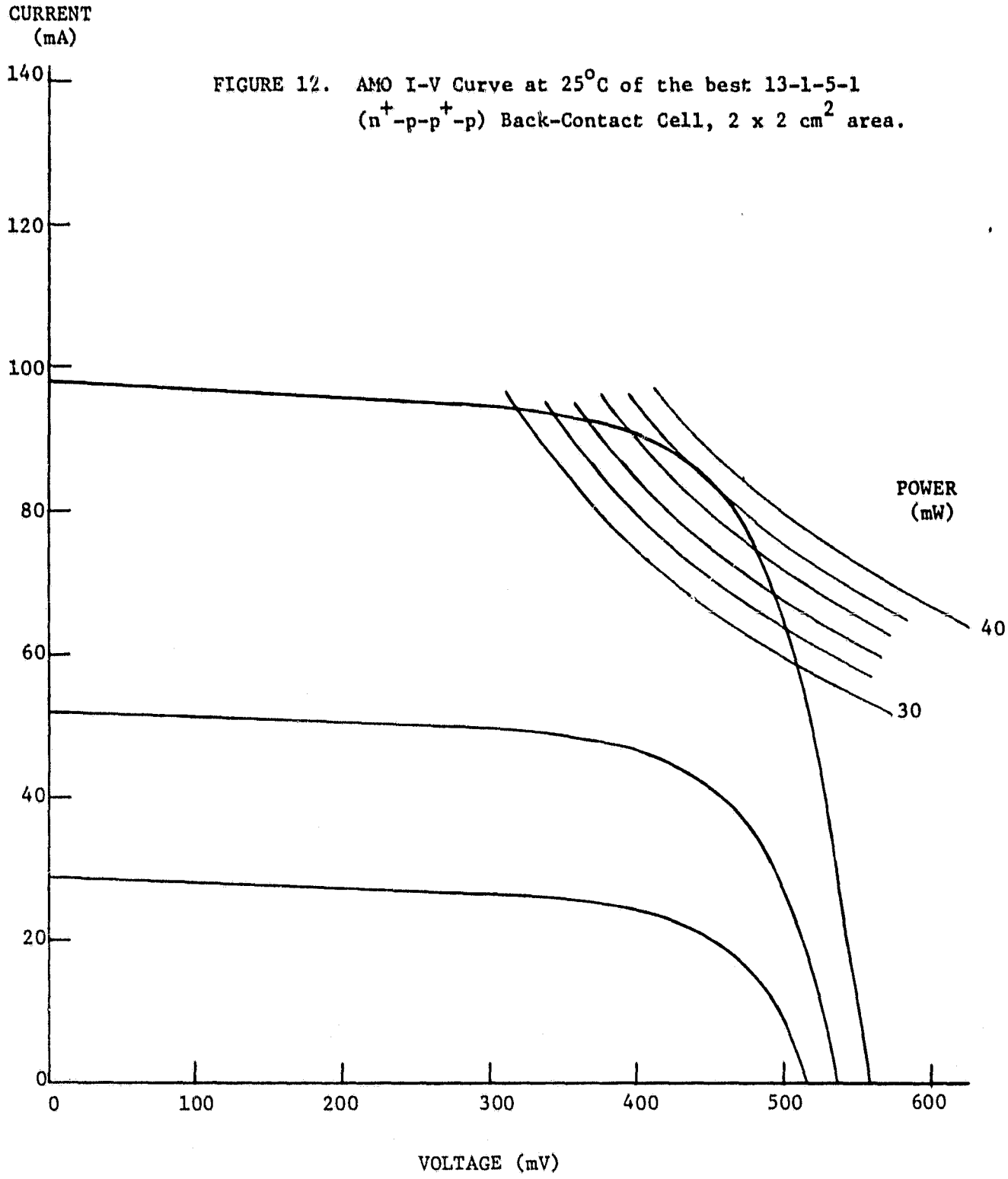

FIGURE 12. AMO I-V Curve at 25°C of the best 13-1-5-1 (n^+-p-p^+-p) Back-Contact Cell, 2 x 2 cm^2 area.

a short-circuit current density of 34.5 mA/cm^2. The gain in efficiency was clearly attributable to the expanded n^+-region.

The previous experiment was repeated using 5 Ω-cm float zone silicon thinned to a thickness of 50-60 μm. Figure 13 shows the I-V characteristics of the best cell fabricated in this group. The AMO peak power and short circuit current density were measured to be 64 mW (11.7% efficiency) and 36.5 mA/cm^2, respectively. The increase in current is believed to be attributable to the fact that the distances that minority carriers must diffuse before reaching the n^+-p junction has been reduced -- that is, bulk recombination becomes less likely as a minority carrier loss mechanism.

Other Fabrication Efforts - Concurrent with the efforts discribed above, other process modifications directed toward achieving higher efficiency cells were investigated.

There was one attempt to fabricate a tandem junction cell - that is, a cell in which there was an n^+-diffused region on the front. Low efficiencies (<4% AMO) and low short circuit densities (<15 mA/cm^2) resulted, and further work was abandoned because of insufficient time.

Textured cells were fabricated concurrently with planar cells in a number of the experimental lots. In every instance, the planar cells had higher efficiencies than the textured cells, although in an experimental group with 50-60 μm silicon slices, the textured cells had equivalent or slightly greater short circuit current densities ($\simeq$ 36.5 mA/cm^2). There was no attempt to spin on an anti-reflection coating; rather, the silicon dioxide initially deposited on the front surface was left intact. Consequently, optimum optical coupling was not obtained. Fabrication of

FIGURE 13. AMO I-V Curve at 25°C of the best 16-1-21-(n^+-p-p^+-p) Back-Contact Cell

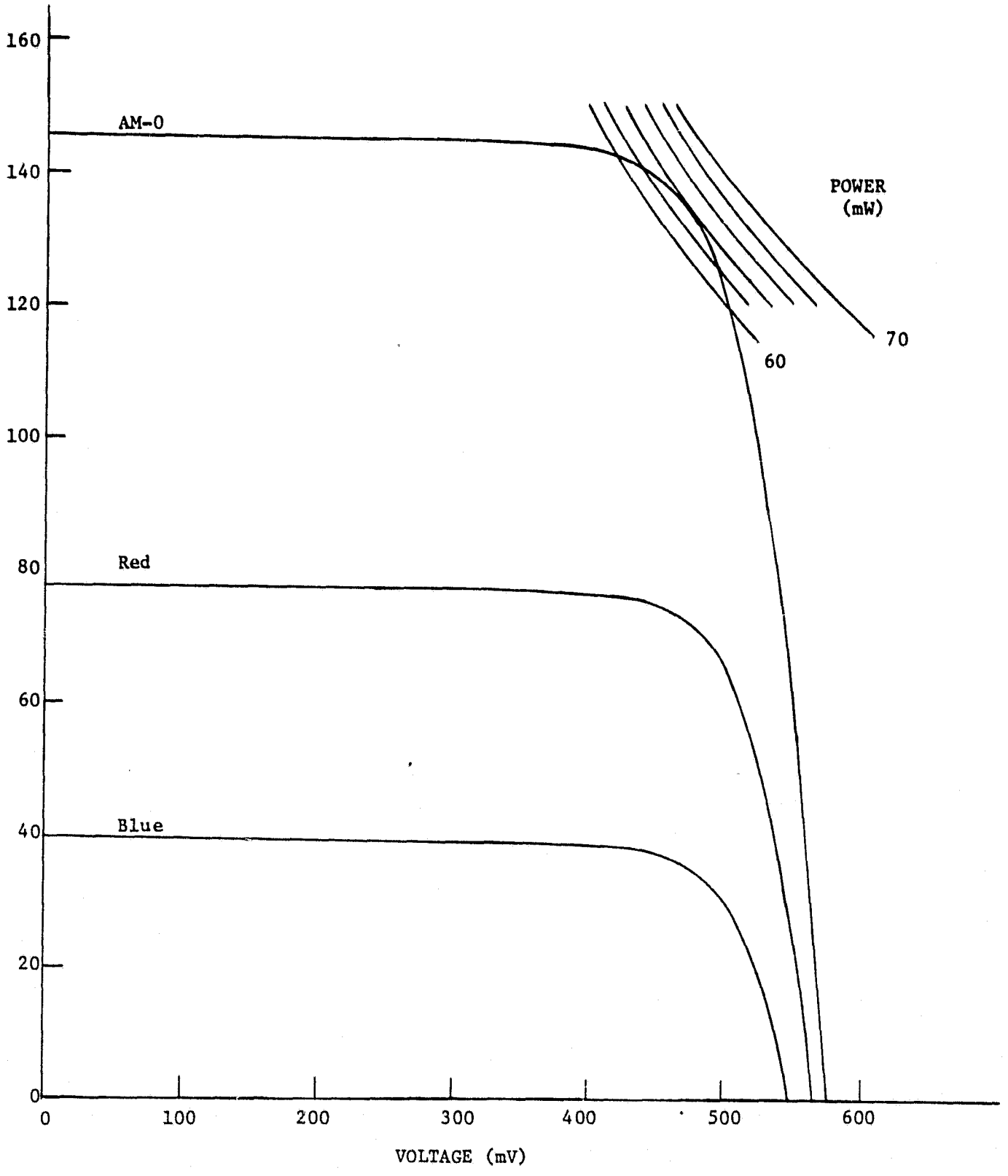

textured cells was plagued by even lower yields than those of planar cells. Because of this, primary efforts were directed towards the fabrication of the planar cells.

In one of the experimental lots, a number of cells were diffused at 950°C in addition to those diffused at 870°C. The purpose was to determine if a variation of the diffusion temperature would affect the cell efficiency. It was found that the higher diffusion temperature caused a substantial decrease in the efficiency.

2.2.2 Production Effort

In the first task, a process was developed that was likely to result in cells having AMO efficiencies between 13 and 14 per cent. This process sequence is seen in Figure 6 . The goal of the second task was to fabricate 48 cells with efficiencies in the 13-14% range. The strategy employed was to fabricate a sufficiently large number of cells such that the top of the distribution would provide the required cells.

During the task one efforts, a major problem that was encountered was misalignment of the back metallization and diffusion regions due to faulty masks. For the task two efforts, this problem was corrected.

Four lots of cells were begun, each lot consisting of 12 to 13 wafers. The potential number of cells was ≃ 300. In the first two lots, few cells survived the processing. Of those that did survive, the process was found to be capable of producing cells of acceptable efficiency (≃ 9% AMO with a non-optimized SiO_2 anti-reflection coating). Fabrication problems severely reduced yield - specifically, major problems were encountered in photolithography and silver plating. The photolithography had to be

repeated several times, with substantial breakage occurring each time. Breakage occurred at silver plating because of inadequate fixturing for this step.

Measures were adopted to reduce the losses at each of these steps, and, in the final lot fabricated, a total of 19 cells out of 72 reached test. No cells having efficiencies in excess of 12% were fabricated. Most of the cells that reached test had some shunting in the I-V characteristics. On examination of the back Al-alloyed region, it was observed that aluminum had flowed across the oxide on top of the p-region and had come in contact with the n^+ diffused region.

No further attempts were made to fabricate cells because solution to the fabrication difficulties would require efforts beyond the time and funding left in the program.

3.0 Summary and Conclusions

- It has been possible to successfully fabricate 50 μm-thick coplanar back contact cells with a front surface field (FSF). Efficiencies up to ≈ 12% AMO have been obtained, and even higher efficiencies could be obtained if various recombination losses were reduced.
- Recombination losses at the front surface have been minimized. The primary losses occur at the back p- and p^+- interfaces and within the bulk p-region. Reduction of the interface losses by passivation (p-surface) or by introducing a more effective high-low junction (p^+-p) would significantly increase current collection.
- Computer modeling indicates the extreme sensitivity of the short-circuit current, and, thereby, the efficiency on the bulk lifetime. Consequently, it is expected that the coplanar back contact cell will be a very radiation sensitive device. To minimize this sensitivity, a cell must have a high initial bulk minority carrier lifetime and be as thin as is practical to fabricate (at present, this limit is ≈ 40 μm).
- A front-surface field cell is expected to be less radiation sensitive than the tandem junction cell, since radiation damage in the front surface space charge region will have a minimal effect on the flow of minority carriers away from the front surface.
- Because of the minimal metallization on the rear of the coplanar back contact cell, it is expected that this type of cell will run at cooler temperatures in a space environment. Most long wavelength light will be transmitted through the cell with little absorption.

APPENDIX

Description of Computer Program Used to Model Coplanar Back Contact Cells

A computer program was written to model the diffusion of photogenerated minority carriers in bulk silicon. The diffusion equation can be written as

$$\nabla^2 n - \frac{n}{L_n^2} + \frac{G}{D_n} = 0 \qquad (1)$$

where n is the minority carrier density in excess of the equilibrium value, G is the photogeneration rate, L_n is the diffusion length, and D_n is the diffusion constant. It is assumed that there are no electric fields in the bulk. Our work has been with moderately doped silicon, 1 to 10 Ω-cm, tested under AMO illumination without concentration. Under these conditions the calculation of current based only on minority carrier diffusion is valid.

The diffusion equation is solved using the relaxation method. For this method the carrier density in the silicon bulk is specified at lattice points as shown in Figure A-1. The number of lattice points can be as large as 20 x 20. The diffusion equation can be rewritten as an algebraic equation between nearest neighbor points as shown in Equation 2.

$$\begin{aligned} &(n_{+,o} + n_{-,o} - 2n_{o,o})/\Delta x^2 \qquad (2)\\ &+(n_{o,+} + n_{o,-} - 2n_{o,o})/\Delta y^2\\ &-n_{o,o}/L^2_n + G_{o,o}/D_n = 0 \end{aligned}$$

Equation 2 can be solved for $n_{o,o}$ as

$$\begin{aligned} n_{o,o} = \big|&(n_{+,o} + n_{-,o})\cdot\{1/\Delta x^2\}\\ &+(n_{o,-} + n_{o,+})\cdot\{1/\ y^2\}\\ &+\{G_{o,o}/D_n\}\big|/\{(1/L_n^2) + 2(1/\Delta x^2 + 1/\Delta y^2)\} \qquad (3) \end{aligned}$$

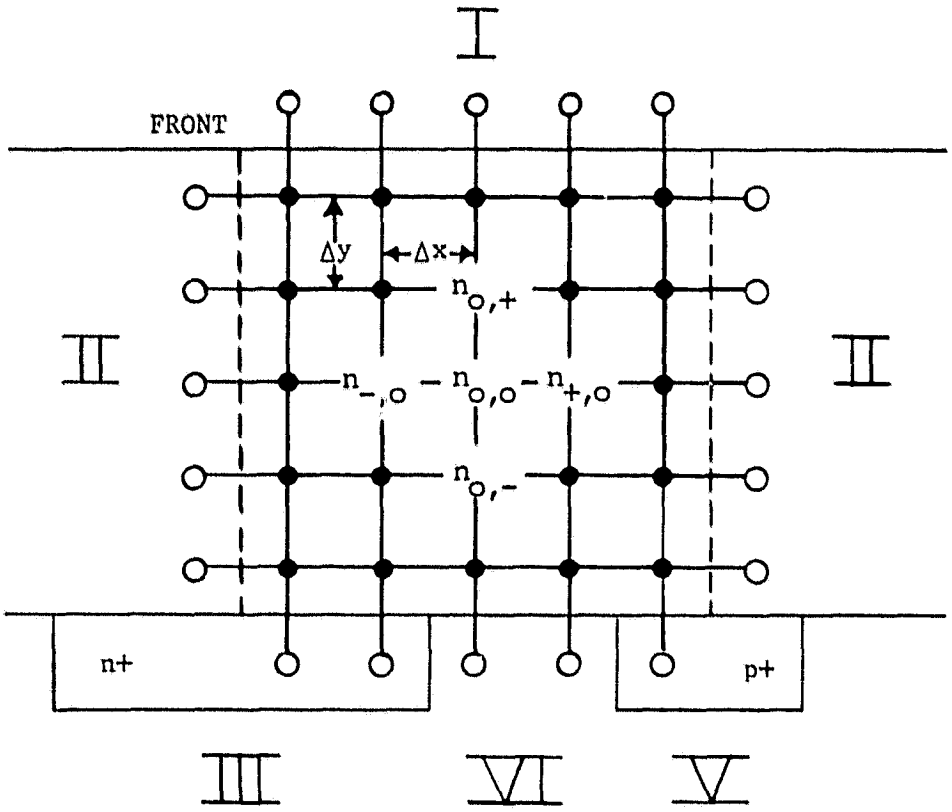

Figure A1. Lattice Point Notation and Boundary Conditions.

Since the calculation of $n_{o,o}$ comprises the inner most program loop, the terms in brackets ,{}, are constants that are calculated only once each experiment in order to speed the computation of Equation 3.

The photogeneration rate at each point, $G_{o,o}$, is calculated by splitting the AMO spectrum into eight wavelength bands spanning the absorption spectrum of silicon (300 nm - 1100 nm). A characteristic absorption constant is used for each band as shown in Table A-1. For each band the number of photons absorbed each Δy thickness is calculated and added to the appropriate $G_{o,o}$.

The relaxation method involves the application of Equation 3 for each point on the lattice. The results (left-hand-side of Equation 3) are stored in a temporary file until all points have been considered. The results are then used for the right-hand-side of Equation 3 and the cycle is repeated. About 400 cycles are required to obtain an accuracy of about 1% in carrier density.

At the boundary one or two nearest neighbors are points outside the silicon. A carrier density is derived for these external points by considering boundary conditions. Referring to Figure A1, regions I, VI, and V are assigned finite surface recombination velocities. Region III is assigned zero carrier density and region II reflects the carrier density on the opposite side of the dashed line. The minority carrier density, n, used for an external point with a given surface recombination velocity, V_s, is given by Equation 4.

$$n = n_{o,o} \cdot (1 - (\Delta y \cdot V_s / D_n)) \qquad (4)$$

The short-circuit current, I_{sc}, is calculated from the points adjacent to the $n^=$ region.

$$I_{sc} = (qD_n/\Delta y)((\Sigma_{k=1}^{N} n_k)/N) \qquad (5)$$

In Equation 5, N is the number of points adjacent to the n^+ region and q is the unit of charge.

TABLE A-1

Photon Flux and Absorption Constant For AMO

Wavelength Band (microns)	Photon Flux ($/cm^2 sec$)	Absorption Coefficient (/cm)
.3 - .39	.17E17	.11E7
.4 - .49	.41E17	.23E5
.5 - .59	.49E17	.72E4
.6 - .69	.50E17	.32E4
.7 - .79	.47E17	.15E4
.8 - .89	.43E17	.64E3
.9 - .99	.40E17	.22E3
1.0 -1.09	.35E17	.30E2

REFERENCES

1. M.D. Lammert and R.J. Schwartz, "The Interdigitated Back Contact Solar Cell: A Silicon Solar Cell for Use in Concentrated Sunlight", IEEE Trans. on Electron Devices, Vol. ED-24, No. 4, April, 1977.

2. B.G. Carbajal, "High Efficiency Cell Development", JPL Report DOE/JPL 954881-79-5, p. 9, February 1979.

3. J. Wohlgemuth and A. Scheinine, "Silicon Solar Cell Optimization", Technical Report AFWAL-TR-80-2059, June 1980.